Polymer Chemistry

Check for updates

Long-chain polyamide covalent adaptable networks based on renewable ethylene brassylate and disulfide exchange†

Charalampos Pronoitis, [ID] Minna Hakkarainen [ID] and Karin Odelius [ID] *

Conventional thermosets cannot be recycled once they reach their end-of-life creating unavoidable waste. Covalent adaptable networks (CANs) are a promising circular solution as they can be reprocessed by conventional techniques employed for processing thermoplastics. In this work, strong and chemically resistant, long-chain polyamide (PA) CANs were developed by introducing intrinsically reactive disulfides in PA networks. Following a solvent-free strategy and utilizing ethylene brassylate, a renewable cyclic diester, our approach brings together the high strength and chemical resistance of long-chain, crosslinked PAs with the reprocessability of dynamic networks in a sustainable fashion. The structure of the PA CANs was elucidated by X-ray diffraction analysis, and the effect of the disulfides on the thermal, mechanical, viscoelastic and dynamic properties was evaluated. The PA CANs had high gel content (86–98%) and they were reprocessable over three grinding-compression molding cycles, retaining their strength (15–20 MPa), crosslink density and gel content. They exhibited rapid stress relaxation with relaxation times as low as 1.06 s and were healable within 5 min. The long-chain PA CANs are easy to prepare and feature several elements of sustainable materials design, highly valued in plastics' circular economy.

Introduction

Unlike thermoplastics that can be recycled and/or reprocessed when they reach their end-of-life, the development of circular thermosets is more challenging. Thermosets reach their end-of-use once they are damaged, as the permanently crosslinked network does not allow reprocessing by conventional techniques, and incineration, landfill or use as lower value additives commonly follow. Associative covalent adaptable networks[1] or vitrimers[2] have emerged as a promising solution to the challenge of achieving recyclable thermosets. Associative CANs are thermally reprocessable and chemical recycling of the pristine synthons is possible in certain cases. Their principle is the activation of exchange reactions between dynamic bonds that overall keep the crosslink density of the network constant, but allow it to flow and rearrange its topology at high temperature. Thus, CANs meld the features of classical thermosets such as chemical resistance and dimensional stability with reprocessability, and in some cases self-healing ability and chemical recycling,[2–7] all highly attractive features for many applications.[8]

Department of Fibre and Polymer Technology, KTH Royal Institute of Technology, Teknikringen 56-58, 100 44 Stockholm, Sweden. E-mail: hoem@kth.se
†Electronic supplementary information (ESI) available. See DOI: 10.1039/d1py00811k

Polyamide (PA) networks have rarely been reported, let alone PA networks with exchangeable bonds. This lack of PA CAN examples could partly be due to the harsh conditions required for the synthesis of PAs and the difficulty to combine a sensitive dynamic motif in the same synthetic protocol. However, fusing the high mechanical strength, thermal and chemical resistance of PAs in a reprocessable network is an intriguing route towards high-performance, sustainable materials. Specifically, long-chain PAs, that is PAs containing aliphatic chains with more than 10 $-CH_2-$ units,[9] are of particular interest not only from an application aspect but also fundamentally due to their structural similarity to polyethylene.[10] Importantly, long-chain PAs are usually derived from fatty acids and/or their derivatives,[11–15] and such systems have been reported to be reprocessable and to exhibit self-healing ability and shape-memory behavior. In systems that are designated as long-chain, the long aliphatic chains hold a critical role both for the design of the structure and the macroscopic properties, and for the dynamic response. To prepare such systems, elegant and efficient synthetic routes have been followed, however, they involved some complex synthesis and purification of precursors, use of transition metal catalysts and/or solvents and toxic reagents for the polymerization or crosslinking.[16–19]

Since the seminal work of Leibler and coworkers,[20] a multitude of different bonds, namely esters,[21,22] disulfides,[23,24] imines,[25,26] urethanes[27,28] and boronic esters,[29,30] have been

This journal is © The Royal Society of Chemistry 2021

employed for the design of reprocessable networks. Seeking for a simpler and more sustainable alternative towards long-chain PA CANs, we focused on disulfides as an intrinsically reactive bond,[31,32] that can be activated under mild conditions.[33] Disulfides have been incorporated into urea,[34] urethane,[23,35,36] ester[4,37] and epoxy-based[38–40] networks, and have been combined with renewable building blocks such as diacids (succinic, adipic, sebacic),[4] castor oil[24,41] and epoxidized soybean oil,[42] leading to high-performance thermosets with impressive results regarding the ease of reprocessability and retainment of the mechanical properties after several reprocessing cycles.

Our aim was to develop biobased, long-chain PA networks that would combine the high mechanical strength and chemical resistance of PAs with the malleability of associative CANs. The long aliphatic chains should endow flexibility to the network and affect its dynamic character, enabling fast relaxation. We hypothesized that a simple and straightforward route to achieve such a system would be by leveraging a solvent-free, ring-opening aminolysis-condensation/crosslinking strategy of renewable ethylene brassylate,[43,44] and the fast disulfide exchange.[4,23,39] The dynamic character of the resulting long-chain PA network was verified by stress relaxation analysis and the material was thermally reprocessable over three grinding-compression molding cycles without deterioration of its properties.

Experimental

Materials

Ethylene brassylate (EB, 95%), tris(2-aminoethyl)amine (TAEA, 96%), 2,2′-(ethylenedioxy)bis(ethylamine) (EDOBA, 98%) and hexamethylenediamine (Hex, 98%) were purchased from Sigma-Aldrich. 1,5,7-Triazabicyclo[4.4.0]dec-5-ene (TBD, 97%) was purchased from ChemScence. Cystamine (Cys) was prepared from cystamine dihydrochloride (98%, AmBeed) as previously described.[23] 1,1,1,3,3,3-Hexafluoropropan-2-ol (HFIP, 99%) was purchased from Apollo Scientific, UK. Chloroform-d (CDCl₃, 99.8%) was purchased from VWR. All reagents were used as received without any further purification.

Preparation of the PA CANs. Networks with different Cys : TAEA molar ratios were prepared, keeping the total ester : amine ratio constant to 1. The samples are named as CysXX, where XX denotes the relative molar amount of cystamine (Cys) compared to TAEA. A typical procedure is described for Cys50; Cys (0.450 g, 0.00296 mol), TAEA (0.432 g, 0.00296 mol) and TBD (0.205 g, 0.00148 mol, 5 mol% to total –NH₂) were added into a 10 mL scintillation vial, which was gently heated with a heat gun until TBD was fully dissolved and the color of the solution turned yellowish-orange. The solution was cooled down to room temperature and EB (2 g, 0.0074 mol) was weighed in the vial. The mixture was thoroughly vortexed, poured in a disposable aluminium pan and placed in an oven at 100 °C for 18 h, followed by 18 h at 140 °C. All samples were stored in a desiccator when not in use.

Characterization

Nuclear magnetic resonance spectroscopy (NMR). ^{1}H NMR spectra were recorded with an Avance 400 spectrometer at 400 MHz, at 298 K and the signals were referenced against the chemical shift (δ) of the residual CHCl₃ in CDCl₃ (7.26 ppm). Data were processed with MestReNova v. 9.0 software.

Fourier transform infrared spectroscopy (FTIR). A PerkinElmer Spectrum 2000 spectrometer with a single reflection-attenuated total reflectance accessory was employed to record the FTIR spectra of the networks. The recording range was 4000–600 cm^{-1} with a 4 cm^{-1} resolution. FTIR data were processed with PerkinElmer Spectrum™ 10 software.

Differential scanning calorimetry (DSC). The thermal properties of the PA CANs were analyzed by DSC with a Mettler Toledo DSC 1 instrument. Typically, 8–10 mg of sample were loaded in aluminium crucibles, and subjected to two heating and one cooling scan from −80 to 120 °C, with a 10 K min^{-1} temperature ramp, under 50 mL min^{-1} N₂ flow. The glass transition (T_g) and melting (T_m) temperatures are reported as the midpoint of the glass transition and the maximum of the melting peak, respectively, from the second heating scan. The values reported are averages of triplicate measurements.

Thermal gravimetric analysis (TGA). The thermal stability of the PA CANs was evaluated by TGA with a Mettler Toledo TGA/DSC 1 instrument under N₂ atmosphere (50 mL min^{-1}). The samples were loaded in alumina crucibles and tested between 50–600 °C with a 10 K min^{-1} heating ramp. DSC and TGA data were analyzed by Mettler Toledo STAR^e v. 15.00 software.

Rheology. Rheological measurements were carried out on a Discovery HR-2 rheometer from TA Instruments, on a parallel plate geometry with disks obtained after grinding and compression molding the pristine materials ($\varnothing$ 25 mm, $T = 1$ mm). The disk of the EDOBA50 was punched directly from the as-cured network using a cutting die. The linear viscoelastic region was determined from a strain sweep (100 °C, 1 Hz, 0.01–10% strain, see Fig. S16–S20†). Stress relaxation experiments were performed at the respective temperature using a constant axial force of 1 N. 1% strain was instantly applied and the relaxation modulus (G_t) decay was recorded over time. G_0 was taken at 0.02 s. Each sample was allowed to equilibrate for 10 min at the respective temperature prior to data acquisition. Rheological data were processed with TRIOS software.

X-ray diffractometry (XRD). XRD patterns of the networks were recorded with a PANalytical X'Pert PRO diffractometer with a Cu Kα radiation source ($\lambda = 0.154$ nm). The measurements were carried out at room temperature, at 2θ angle between 0 and 60° with a 0.017° angular step, on a monocrystalline Si sample holder. The materials were grinded into a powder prior to measuring.

Energy-dispersive X-ray spectroscopy (EDS). Elemental analysis of the PA CANs was performed by EDS using a field-emission Hitachi S-4800 scanning electron microscope (SEM) equipped with an X-Max^N 80 mm^2 Silicon Drift detector from Oxford Instruments. The accelerating voltage of the electron beam was 10 kV and the samples were sputter-coated with a

Pt/Pd alloy prior to analysis on a Cressington 208HR unit. Mapping was carried out on at least two different areas of each sample.

Compression molding. The grinded networks were compression-molded with a TP 400 hot-press from Fontune Presses. The grinded samples dispersed in the mold were sandwiched between two PTFE sheets (T = 0.1 mm) and placed in between two stainless steel disks (∅ 23 cm, T = 0.5 cm). This setup was put in the hot-press and left to equilibrate for 2 min under the applied pressure at 160 °C. Then, the pressure was instantly released, reapplied and kept steady for 1 min, and released again. This 1 min venting cycle was repeated two more times before letting the specimens shape under pressure at 160 °C for 20 min.

Tensile testing. The mechanical properties were evaluated according to ASTM D1708 using an Instron 5944 tensile tester equipped with a 500 N load cell, at a crosshead speed of 1 mm min^{-1}. The as-cured films were grinded with a Bosch© TSM6A013B coffee grinder and compression-molded (160 °C, 6 MPa, 20 min) using a custom-made steel mold in dumbbell-shaped specimens (38 mm (L) × 5 mm (W) × 0.8 mm (T), effective gauge length 22 mm). Prior to testing the specimens were conditioned at 23 ± 2 °C and 50 ± 10% relative humidity for 40 h. The results are averages of three repeats. The data were processed with Bluehill® 3 software.

Dynamic mechanical analysis (DMA). The networks were subjected to DMA (Q800, TA Instruments) using rectangular-shaped specimens (7–10 mm (L) × 5 mm (W) × 0.8 mm (T)) cut from the dumbbell-shaped specimens made for tensile testing. Temperature sweeps from −50 to 120 °C (3 °C min^{-1}, 1 Hz, 0.1% strain) were carried out and the crosslink density (v_e) and average molar mass between crosslinks (M_c) were calculated through eqn (1):

$$v_e = \frac{E'}{3RT} = \rho M_c^{-1} \qquad (1)$$

where E' is the storage modulus in the rubbery plateau at the respective temperature T, R is the universal gas constant (8.314 J K^{-1} mol^{-1}), and ρ is the density of the networks calculated through the mass and volume of rectangle specimens thrice (Cys30 0.978 ± 0.007 g cm^{-3}; Cys40 0.977 ± 0.020 g cm^{-3}; Cys50 1.009 ± 0.040 g cm^{-3}; Cys60 1.039 ± 0.041 g cm^{-3}; EDOBA50 1.096 ± 0.075 g cm^{-3}). DMA data were analyzed by TA Universal analysis software (v. 4.5).

Gel content. A piece of each network was weighed in a scintillation vial and swelled in HFIP for 24 h. The dissolved fraction was filtered out and the remaining solids were dried at 80 °C under vacuum until constant mass was reached. The gel content was calculated through eqn (2):

$$\text{Gel content} = \frac{m_d}{m_0} \times 100\% \qquad (2)$$

where m_d and m_0 are the mass of the dried and initial sample, respectively. The measurements were repeated three times for each sample.

Chemical resistance of the PA CANs. Specimens from Cys40 that was already hot-pressed once, were immersed in each solvent for 24 h. After, the specimens were washed with copious amounts of acetone and dried at 100 °C under vacuum. The mass loss was recorded for each specimen in the respective solvent, see Table S2.†

Results and discussion

Structure, thermal and viscoelastic properties of the PA CANs

Biobased long-chain PA associative CANs were successfully prepared by incorporating exchangeable disulfide (S–S) bonds in PA networks. The molar ratio between the amine-containing reactants (cystamine and tris(2-aminoethyl)amine, TAEA) was varied to achieve CANs with different S–S content and cross-link density, and to evaluate their influence on the thermal properties, mechanical properties, and ability of the dynamic networks to rearrange their topology. Reference networks with non-dynamic bonds were also prepared for comparison reasons. The general strategy towards the long-chain PA associative CANs is presented in Fig. 1.

To achieve the synthesis of the PA CANs, we screened the reaction conditions that promoted an efficient ring-opening aminolysis-crosslinking reaction between EB, Cys and TAEA. For the neat EB/TAEA system, the reaction proceeds efficiently at 100 °C under basic catalytic conditions (4 mol% of TBD to –NH$_2$), yielding PA networks with high gel content (~93%).[44] When the same reaction conditions were applied to the EB/Cys/TAEA mixtures with varying the Cys : TAEA molar ratio (20 : 80 to 80 : 20), networks with lower than expected gel content (89–81%) were obtained and the FTIR spectra showed some unreacted EB monomer left, Fig. S1.† Higher gel content values could not be achieved by increasing the temperature to 120 °C or by extending the reaction time (48 h) at 100 °C. Side-reactions involving Cys were excluded as the compound was stable at high temperature and in basic conditions, Fig. S2.† The lower gel content was a result of replacing part of the trifunctional TAEA with difunctional Cys, therefore reducing the crosslink density of the networks (*vide infra*).

Hence, to ensure the successful incorporation of Cys in the PA networks, a two-step procedure was implemented along with a slightly higher catalyst loading (5 mol% to total –NH$_2$). The first step was performed at 100 °C for 18 h and ring-opening of the majority of EB took place. In a second step, the reaction temperature was increased to 140 °C for additional 18 h to drive the aminolysis reaction further. After the two-step procedure, the gel content was 98, 94, 90 and 86% for Cys30, Cys40, Cys50 and Cys60, respectively, and elemental mapping showed that sulfur was homogeneously distributed over the network indicating a successful network formation, Fig. S4–S7.† To further prove that most of the monomers have been incorporated into the networks, the dissolved phases, collected after swelling the networks in HFIP, were analyzed by ^{1}H NMR spectroscopy. The ^{1}H NMR spectrum showed that the dissolved fractions consisted mostly of TBD and traces of mono-
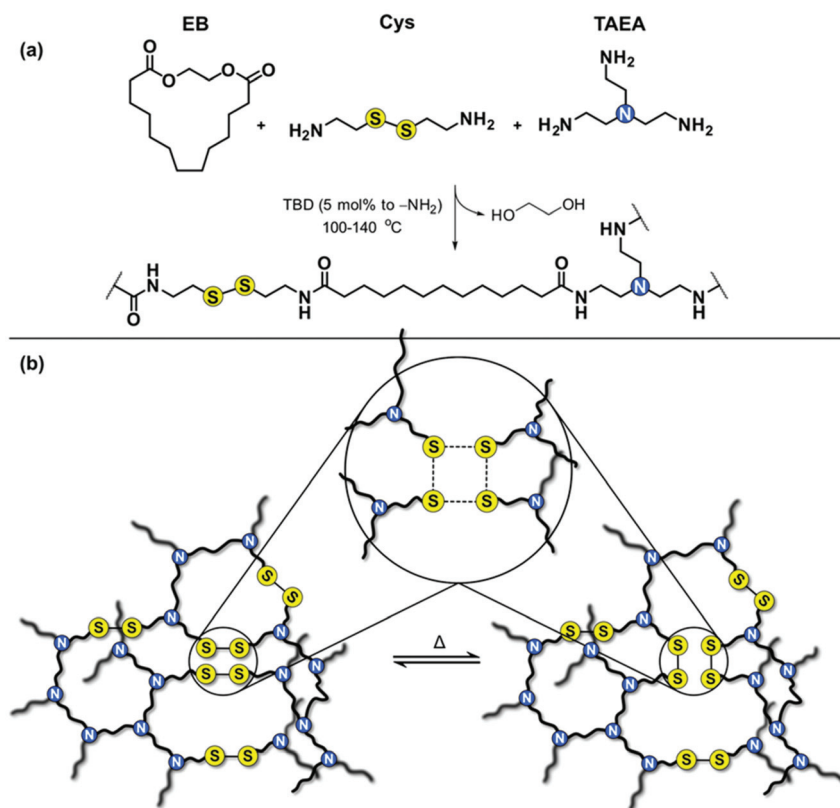
Fig. 1 Synthesis of long-chain PA associative CANs; (a) general reaction scheme and (b) schematic representation of the disulfide exchange in the network.

mers and/or soluble oligomers, Fig. S3.† Hence, to achieve Cys-containing, dynamic PA networks with high gel content, a higher curing temperature and longer reaction time were necessary.

The appearance of the characteristic N–H stretching (3290 cm^{-1}) and the amide I (1634 cm^{-1}) and amide II (1541 cm^{-1}) bands in the FTIR spectra of the resulting materials, concomitantly with the disappearance of the C=O stretching of EB (1736 cm^{-1}), confirmed the formation of the amide bonds and the successful preparation of the PA networks, Fig. 2a. The presence of consecutive ester units in the network resulting from ring-opening oligomerization of EB cannot be excluded,[44] but no signal in the 1740–1720 cm^{-1} range (ester C=O stretching) was observed in the FTIR spectra. The networks were thermally stable at least up to 260 °C with $T_{d,5\%}$ values lower than those of pure PA networks,[44] Fig. S8.† The lower thermal stability is a consequence of the presence of thermally sensitive S–S bonds as confirmed by the observed decrease of the $T_{d,5\%}$ values with increasing the Cys content, namely 293, 284, 276 and 259 °C for Cys30, Cys40, Cys50 and Cys60, respectively. These $T_{d,5\%}$ values are similar to those reported for other aromatic or aliphatic disulfide-based urethane and epoxy associative CANs.[23,40,42]

The networks were semicrystalline and their thermal and viscoelastic properties were altered by the increasing content of Cys as proven by DSC and DMA, Fig. 2b–d, Table 1. The

general trend observed by DSC was a decrease of T_g and an increase of T_m with increasing the Cys content. This trend can be explained when considering that the increasing Cys content resulted in lower crosslink density (v_e) and larger molar mass between crosslinks (M_c), Table 1. Consequently, the higher chain mobility in the network was reflected on the decreasing T_g from 28 to 16 °C for Cys30–60, respectively. The crystallinity observed was attributed to the aliphatic chains of the amide strands, i.e. the linear macromolecular segments connected to the crosslinks. The increase of T_m with higher Cys content (75–81 °C) was accompanied by higher enthalpy of fusion (ΔH_m) which is congruent with the behavior observed for other linear, aliphatic oligoamides of PA-10,10 exhibiting higher T_ms and degree of crystallinity at higher molar mass, but also higher T_m values than the PA networks (118–188 °C).[45] Four factors account for the lower T_m values of the PA networks compared to those of linear oligoamides: (i) the presence of crosslinks in the PA networks, (ii) the discrepancies in the conformation and crystal structure arising from well-known odd-even effects,[46–49] (iii) the perturbing effect of the amide groups on the crystallization ability of the aliphatic chain,[10] and (iv) the presence of the S heteroatoms disturbing the packing of the aliphatic chains.[15] However, as previously explained, replacing TAEA with Cys entails higher degree of chain freedom as the amide strands became longer and facilitated the development of H-bonding between the amide groups. Further, due to
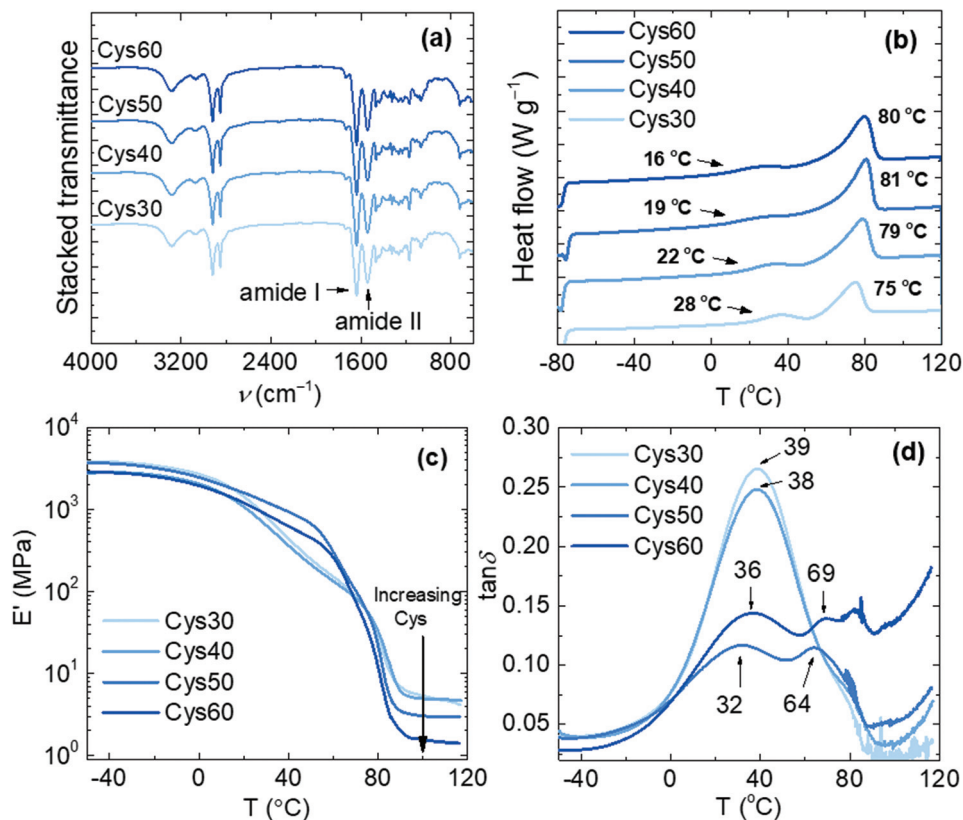
Fig. 2 Characterization of the PA CANs; (a) FTIR spectra, (b) DSC traces of the 2nd heating scan and (c), (d) E' and $\tan\delta$, respectively, from DMA analysis.

Table 1 Thermal and viscoelastic properties of the PA CANs and the EDOBA50 reference network

Network	$T_{g,\,DSC}$[a] (°C)	$T_{g,\,DMA}$[b] (°C)	T_m (°C)	ΔH_m (J g^{-1})	E''^c (MPa)	ν_e[d] (mol m^{-3})	M_c[d] (g mol^{-1})
Cys30	28 ± 0.1	40 ± 3	75 ± 0.6	17 ± 0.3	5.0 ± 0.3	540 ± 33	1820 ± 110
Cys40	22 ± 0.3	38 ± 0.8	79 ± 0.7	18 ± 6	5.0 ± 0.2	538 ± 21	1820 ± 69
Cys50	19 ± 0.3	35 ± 3	81 ± 0.6	27 ± 1	3.8 ± 0.9	409 ± 92	2550 ± 560
Cys60	16 ± 0.1	39 ± 2	80 ± 1	25 ± 1	1.6 ± 0.4	170 ± 39	6320 ± 1430
EDOBA50	11 ± 0.8	16 ± 2	84 ± 0.8	33 ± 2	3.4 ± 0.4	364 ± 46	3040 ± 360

[a] Obtained from the 2nd heating scan. [b] Maximum of $\tan\delta$. [c] Storage modulus in the rubbery plateau. [d] Calculated through eqn (1).

the low electronegativity difference between S and H, S is considered a weak H-bonding partner however, it does participate in H-bonding,[50–52] and/or generally in secondary interactions. Hence, when higher number of S atoms were available in the network, the possibility of H-bonding increased and as a consequence the T_m increased. For comparison, pure EB/TAEA networks and linear EB homopolymers exhibited a T_m of 67 and 69 °C, respectively.[44,53] Keeping the 50 : 50 ratio of diamine : TAEA but replacing cystamine with 2,2′-(ethylenedioxy)bismethylamine (EDOBA) or hexamethylenediamine (Hex) resulted in networks (EDOBA50 and Hex50) with T_m = 85 and 68 °C, respectively. The T_m of Hex50 is much lower than EDOBA50 and Cys50, both of which contained additional heteroatoms participating in secondary interactions and therefore increasing the T_ms of the networks. Hex50 had also a

second T_m = 123 °C due to the additionally crystalline macromolecules formed with hexamethylenediamine between the crosslinks. Full characterization of EDOBA50 and Hex50 are provided in Table S2, Fig. S21–S23.†

The viscoelastic properties of the networks were influenced by the Cys content as shown by the decreasing storage modulus in the rubbery plateau region, Fig. 2c. This drop in the elastic response is consistent with more loosely crosslinked networks exhibiting higher M_c, and corresponds with the values calculated here, M_c increased from 1820 g mol^{-1} for Cys30 to 6320 g mol^{-1} for Cys60, Table 1. The T_g values (40–35 °C) taken from the maxima of the $\tan\delta$ curves, correlated with the trend in DSC, although for Cys60 (39 °C) a higher value than Cys50 (35 °C) was recorded, Table 1. It is noteworthy that if the maxima of the E'' curves are considered

as the T_g, the same decreasing trend with higher Cys content and the same phenomenon of $T_{g,\,Cys60} > T_{g,\,Cys50}$ are observed, Fig. S9.† Further, some of the tested samples of Cys50 and Cys60 showed more than one maximum in the tan δ curves, Fig. 4c, Fig. S10.† Recognizing the origin of multiple peaks in tan δ curves is challenging,[54] but the two maxima observed here could be explained based on subtle discrepancies in the local environment of the amide strands and in the concentration of the bulkier S atoms. Depending on their proximity to the crosslink points, different parts of the amide strands would exhibit different degrees of chain freedom, lower for those found closer to a crosslink site and higher for those farther away. Given the high sensitivity of DMA in detecting structural changes, it is possible that those different regions reflected on the tan δ curves as two maxima. The higher T_g of Cys60 than Cys50 can be rationalized on the basis of the higher number of bulkier S atoms in the former. In fact, although a lower crosslink density is usually regarded as a definitive parameter that will decrease the T_g of a network, there are cases for which this rule is not met.[55,56] The expected presence of network defects (loops, dangling chains) could also contribute to above-described effects.[57,58]

The crystalline structure of the PA networks was elucidated by XRD analysis. All of the networks displayed a single diffraction peak at 2θ 21.4°, and the amorphous halo was observed only Cys30 and Cys40, Fig. 3. The 21.4° peak, due to the (110) crystal plane, is characteristic of the orthorhombic crystal lattice adopted by long-chain hydrocarbons,[59] polyethylene-like polyesters,[60] and long-chain polyamides,[10] polyacetals and polycarbonates.[61] Crystallization in the orthorhombic system is further supported by the characteristic –CH₂– scissoring and rocking vibrational modes in the FTIR spectra at 1466 and 720 cm⁻¹, respectively.[10,62,63] The EDOBA50 control network and a network prepared only with EB and TAEA, featured exactly the same XRD patterns as the Cys-containing dynamic networks, yet the peak was slightly shifted at 21.7°. This difference in the position of the peak from 21.7 to 21.4°, indicates a

slightly larger unit cell for the PA CANs specifically, a distortion of the a and b unit cell parameters, due to the addition of the larger S–S groups compared with the –CH₂– groups. Similar behaviour has been reported for long-chain PAs containing sulfide bonds.[15] In fact, applying Bragg's law it is seen that the distance between the crystal planes (d) slightly increased from 41 to 41.5 Å (see ESI† for calculations). The absence of peaks at 2θ > 22–23° that have been reported for other long-chain aliphatic PAs[10] or EB homopolymers[64] implies the absence of higher-order organization of the amide strands along the c-axis of the crystalline cells. Since the number of carbons in EB are 13 (PA-X,13), the amide strands can be considered long-chain,[9,43] but with high density of amide groups (133.3 per 1000 –CH₂– units). Mecking et al.[10] suggested that when the density of amide groups is higher than ~50 per 1000 –CH₂– units, the orthorhombic system is not favored anymore due to the increased cohesion energy from the pronounced H-bonding. The reason why the orthorhombic system was maintained in the presented PA networks is not clear but we speculate that, despite the higher amide density compared with other long-chain PAs[9] and the presence of the S heteroatoms participating in secondary interactions, the crosslinks could create an inverse "locking" effect resulting in the retainment of the orthorhombic crystal structure. Through several studies, the structure and properties of thermoplastic, long-chain PAs and their relation with purely linear polyethylene are now more fundamentally understood.[9,65–68] Although the focus here was on finding a simple and sustainable pathway towards reprocessable PA networks, the above results can be the basis for future work aiming to develop crosslinked PAs with even longer aliphatic segments. The elucidation of the specific effects of the crosslinks and the presence of heteroatoms on the crystal structure, thermal, mechanical and viscoelastic properties of such networks would be valuable for a deeper understanding of the structure–property relationships.

Dynamic, mechanical properties and reprocessability of the PA CANs

Stress relaxation experiments proved the dynamic character of the PA networks. 1% strain was instantly applied and the decrease of the relaxation modulus (G_t) was monitored until it reached 0.37 (1/e) of its initial value (G_0), according to Maxwell's model for viscoelastic fluids,[69] eqn (3):

$$\frac{G_t}{G_0} = e^{-\frac{t}{\tau}}. \tag{3}$$

Disulfide exchange was proposed already in 1946 as a plausible mechanism accounting for the stress relaxation of polysulfide rubbers.[70] Thanks to the fast exchange reaction, various disulfide-based CANs have displayed short relaxation times in a range of temperatures.[4,23,39] In this system, the long aliphatic chains and the increasing M_c with higher Cys content should impact the relaxation times, in accordance to the impact on the thermal, viscoelastic and mechanical properties (vide infra).
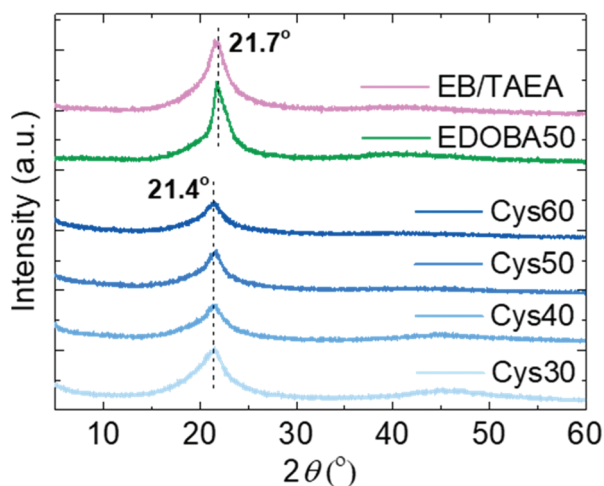

Fig. 3 XRD patterns of the PA CANs and the control networks.

To test our hypothesis, we selected Cys60 which had the highest M_c, and tested its response to stress relaxation at different temperatures, Fig. 4a and b. Cys60 fully relaxed the applied stress as a result of the disulfide exchange and the relaxation time (τ) decreased from 6.6 to 1.06 s, shorter as the testing temperature increased from 80 to 105 °C. At 105 °C τ was 1.06 s indicating an extremely rapid relaxation and a very easy activation of the disulfide exchange reaction, similar to other disulfide-based CANs containing flexible polysulfide or polyether segments.[71,72] In fact, the very fast relaxation is likely ascribed to the highest M_c of Cys60 (6320 g mol⁻¹) as the long flexible amide strands are expected to enable longer-range chain mobility compared to the other more densely cross-linked PA CANs. Hence, the exchange between disulfides is promoted as the probability of two adjacent groups meeting is increased. As the network was above its T_m (80 °C) during testing, the molten state contributed to the higher chain mobility and therefore to the low τ values. However, even at temperatures lower than the T_m (70 °C), full stress relaxation was observed in reasonably short times (87 s), while at a temperature higher than 105 °C the relaxation time was shorter than 1 s, Fig. S11.† It should be noted that the presence of TBD may have a salutary effect on the exchange reaction between disulfides,[39,72–74] although it should not be the dominant factor for it. The system followed an Arrhenius-like behavior as shown by plotting τ against temperature, Fig. 4b. The acti-

vation energy (E_a) was calculated to be 76.7 kJ mol⁻¹, a value comparable to some other disulfide-based CANs,[23,36,39,71] although it can vary significantly both for the aliphatic and aromatic disulfide exchange reaction.[4,24,40] The dynamic character was further proven for all the PA CANs with different content of Cys, and the EDOBA50 control network was tested under the same conditions. All of the PA CANs were capable of fully relaxing the stress, whereas the EDOBA50 control network showed minimal stress relaxation (G_t/G_0 = 0.8 after 10 800 s), Fig. 4c. The decrease of its relaxation modulus was largely due to the high linear content of the network. For the PA CANs, τ increased from 1.6 to 2986 s with decreasing the Cys content as a direct consequence of the decreasing number of disulfides and the increasing crosslink density. The latter hinders the diffusion of the disulfides to a higher extent in Cys30 and Cys40 compared to Cys50 and Cys60, explaining the difference of the relaxation times. Overall, the observed trend is consistent with the behavior of other associative CANs where the relaxation rate is dictated by the concentration of the exchange-controlling species (either catalyst or self-activated motif) and the crosslink density.[6,22,23]

In an attempt to retain the crosslink density while varying the fractions of dynamic bonds, three reference networks with similar gel content and crosslink densities, yet with varying S–S content were prepared. To do so, a part of Cys was replaced by EDOBA, while the overall diamine : triamine ratio was kept
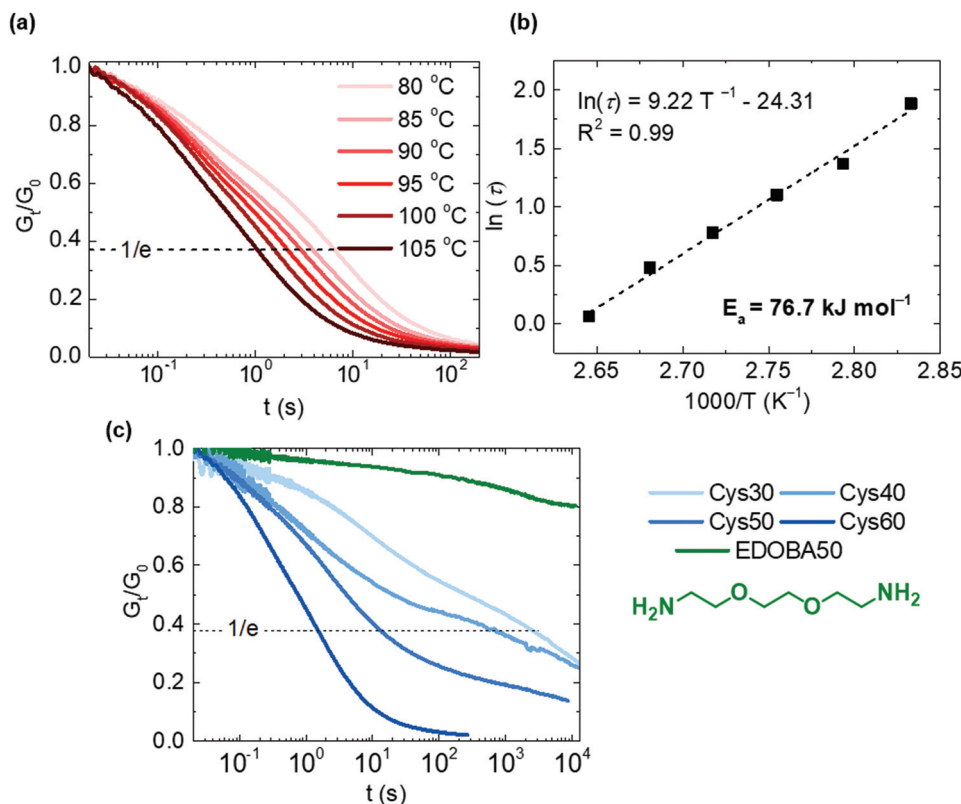

Fig. 4 Dynamic properties of the PA CANs; (a) stress relaxation curves of Cys60 at different temperatures, (b) relaxation times (τ) as a function of the temperature and calculation of the activation energy (E_a) for Cys60 and (c) comparison of the stress relaxation of Cys30−60 at 100 °C.

constant at 50 : 50. Three formulations of EDOBA : Cys were created, namely, 40 : 10, 25 : 25 and 10 : 40, Fig. S12–S15, Table S1.† The dynamic response of these networks was vastly different. The 40 : 10 and 25 : 25 EDOBA : Cys networks did not exhibit full stress relaxation, with G_t/G_0 values at the end of the testing time being 0.75 and 0.43 respectively, reflecting the increasing dynamic bond content. In contrast, the 10 : 40 EDOBA : Cys network having the highest number of dynamic S–S bonds fully relaxed stresses within 28.5 s, a value that is reasonably lower than Cys50 (τ = 14.7 s), Fig. S15.† Overall, the reference networks along with EDOBA50 prove that disulfide metathesis is the mechanism that enabled the stress relaxation to the Cys-containing networks.

The mechanical properties of the PA CANs were evaluated by tensile testing. The networks generally exhibited a rigid profile with high strength, typical of PAs, but without a clear yield point, Fig. 5a. Compared to PA networks made of EB and TAEA (E = 150–330 MPa, σ_b = 7–17 MPa, ε_b = 70–176%),[44] the PA CANs were comparably strong (σ_b = 7–15 MPa) but more rigid, E varied between 350–440 MPa and increased with the Cys content, presumably due to the bulkier S atoms. If compared among them, the strength (σ_b) and strain at break (ε_b) followed the order Cys50 > Cys40 > Cys60 > Cys30 and Cys50 > Cys40 > Cys30 > Cys60, respectively, revealing an intriguing

dual effect of the number of S–S bonds on the mechanical properties. As the content of Cys increased from Cys30 to Cys50, σ_b and ε_b increased as well, but that increment was discontinued for Cys60 which contained the highest number of S–S bonds. As explained previously for the thermal properties, introducing more Cys in the PA CANs increased the M_c and endowed them higher flexibility, resulting in the almost linear increase of σ_b and ε_b going from Cys30 to Cys50. However, the lower bond dissociation energy (BDE)[75] of dialkyl disulfides (277 kJ mol^{-1}) compared to other stronger bonds found in the network, e.g. C–C (BDE $\geq$ 350–360 kJ mol^{-1}), could macroscopically be translated in a higher propensity of Cys60 to break upon exertion of a mechanical force. Putatively, the optimum balance between the beneficial effect of the longer, flexible amide strands on σ_b and ε_b, and the sensitivity of the S–S bonds towards breaking was reached for Cys50, which presented the highest strength and elongation among the PA CANs.

The reprocessability of the PA CANs was demonstrated through three cycles of grinding-compression molding. The disulfide exchange promoted the topological rearrangement of the network and enabled its reformation. The grinded networks were compression-molded for 20 min at 160 °C, under 6 MPa pressure and perfectly consolidated specimens were obtained, Fig. 5b. The reprocessed specimens were subjected to tensile testing and DMA to evaluate their mechanical performance, as well as FTIR and gel content measurements to confirm that their structure remained unaffected during the reprocessing. The properties of the PA CANs for each cycle are summarized in Table 2. No significant loss of the tensile mechanical properties was observed for the reprocessed networks with the σ_b and ε_b values being very similar to the values of the pristine networks, Fig. 5c–f. An exception was Cys50 for which the reprocessed material had lower σ_b and ε_b values compared with the original material (20 MPa, 10% vs. 15 MPa, 5%) yet, with the stress–strain curves over the three reprocessing cycles being almost identical. Additionally, σ_b and ε_b of both Cys40 and Cys50 were higher than the values of Cys60, in line with the previous discussion concerning the effect of the number of S–S on the mechanical properties. The storage modulus in the rubbery plateau remained constant or slightly decreased indicating a constant crosslink density, Fig. S24,† and the gel fraction remained essentially unchanged strongly indicating that no side-reactions or permanent damage took place during reprocessing. The FTIR spectra recorded after each reprocessing cycle corroborated these results showing that the chemical structure of the networks remained unaffected, Fig. S25.† Overall, the characterization of the reprocessed networks proved the efficiency of the S–S as a dynamic motif that enabled the creation of high-performance, fully reprocessable PA CANs without deterioration of their properties.
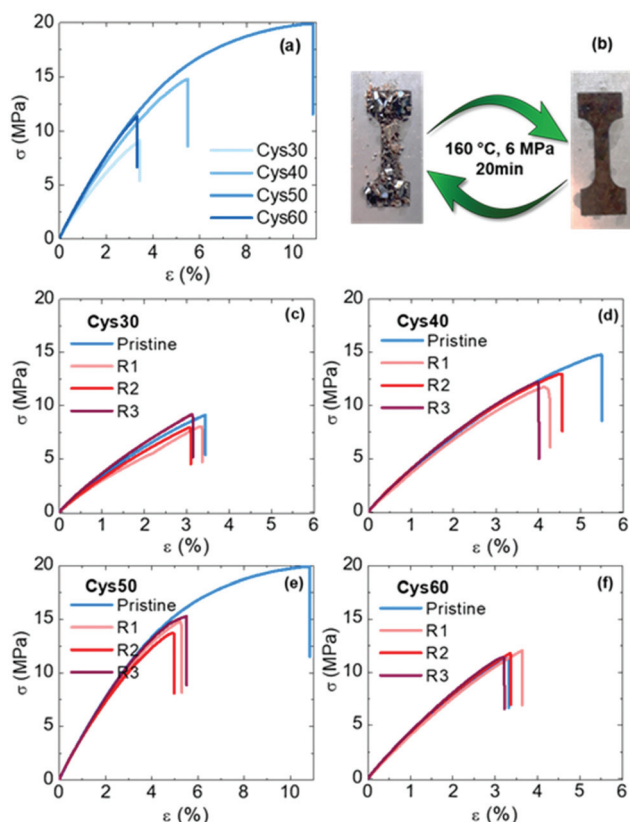

Fig. 5 Mechanical properties of the PA CANs; (a) stress–strain curves of the pristine networks, (b) appearance of a reprocessed sample after compression molding and (c–f) stress–strain curves of the reprocessed CANs.

Healing and chemical resistance of the PA CANs

Disulfide metathesis has been previously exploited as a means to induce (self-)healing to associative CANs.[34,36,76,77] We pre-

Table 2 Mechanical and viscoelastic properties of the PA CANs after three reprocessing cycles (RC)

PA CAN	RC	E (MPa)	σ_b (MPa)	ε_b (%)	E'^a (MPa)	Gel fraction
Cys30	Pristine	348 ± 10	9.1 ± 0.05	3.6 ± 0.3	5.0 ± 0.3	0.98 ± 0.01
	1	321 ± 12	7.7 ± 1.1	3.1 ± 0.5	4.2 ± 1.4	0.96 ± 0.02
	2	348 ± 15	8.0 ± 0.7	3.0 ± 0.2	2.8 ± 0.6	0.97 ± 0.01
	3	380 ± 10	8.7 ± 0.7	3.0 ± 0.2	3.3 ± 1.0	0.95 ± 0.0006
Cys40	Pristine	373 ± 14	14.1 ± 0.8	5.4 ± 0.3	5.0 ± 0.2	0.94 ± 0.05
	1	363 ± 4	11.3 ± 1.2	4.1 ± 0.3	4.7 ± 1.5	0.92 ± 0.04
	2	357 ± 61	11.6 ± 1.4	4.4 ± 0.2	5.4 ± 1.4	0.93 ± 0.03
	3	388 ± 23	11.8 ± 0.9	4.1 ± 0.3	3.9 ± 1.4	0.91 ± 0.01
Cys50	Pristine	400 ± 5	19.6 ± 0.3	10.4 ± 1.9	3.8 ± 0.9	0.91 ± 0.04
	1	409 ± 7	14.7 ± 0.7	5.1 ± 0.3	2.7 ± 1.2	0.94 ± 0.02
	2	412 ± 13	13.5 ± 0.5	4.9 ± 0.2	2.7 ± 0.3	0.89 ± 0.05
	3	409 ± 16	15.5 ± 1.1	5.4 ± 0.07	3.4 ± 1.0	0.87 ± 0.006
Cys60	Pristine	435 ± 15	11.2 ± 1.9	3.3 ± 0.3	1.6 ± 0.4	0.86 ± 0.01
	1	440 ± 23	12.3 ± 1.2	3.6 ± 0.5	2.2 ± 0.2	0.90 ± 0.01
	2	431 ± 32	12.3 ± 1.9	3.9 ± 1.1	2.0 ± 0.1	0.88 ± 0.01
	3	418 ± 9	15.4 ± 0.9	5.2 ± 0.5	2.2 ± 0.3	0.81 ± 0.06

^{a} Storage modulus in the rubbery plateau.

sumed that despite the rigidness of the PA networks due to the H-bonding, the disulfide exchange could be thermally activated to facilitate networks that are healable. As a proof of concept, a disk of Cys60 (∅ 23 mm, T = 3 mm) was cut in half with a sharp blade and the two cut surfaces were merged together while heated over a conventional heat gun operating between 150–200 °C. Already after 5 min of heating and keeping the cut surfaces pressed against each other, the as-healed disk could withstand a 2 kg load hung perpendicularly to the cut, Fig. 6. Thus, the disulfide exchange occurring at the interface of the two pieces of the disk resulted in a robust healing. Although this protocol was not optimized, it provides tangible proof that the PA CANs were healable, a highly valued property of the thermosets of the future that should ideally regain their function quickly after damage, without compromising the rest of their structure.

Finally, when associative CANs are placed in a good but non-reactive solvent they behave as conventional thermosets, they only swell and they do not dissolve. To evaluate the chemical resistance and stability of the PA CANs, samples from Cys40 that were already hot-pressed one time, were tested against an array of solvents, Fig. 7, Table S3.† Infused with the notable chemical resistance of PAs and balanced with the dynamic nature of disulfides, Cys40 showed minimal mass loss (≤5%) in most solvents. In DMF, DMSO and 1 M NaOH, partial swelling and coloration of the solutions was observed and associated to 7–8% mass loss, while in DCM, a maximum of 12% mass loss was measured. As PAs are well-known for their particular resistance against solvents due to their polar nature, the fact that they were already reprocessed one time prior to the solvent-resistance test, likely contributed to the measured mass loss. Overall, the test indicated that the PA
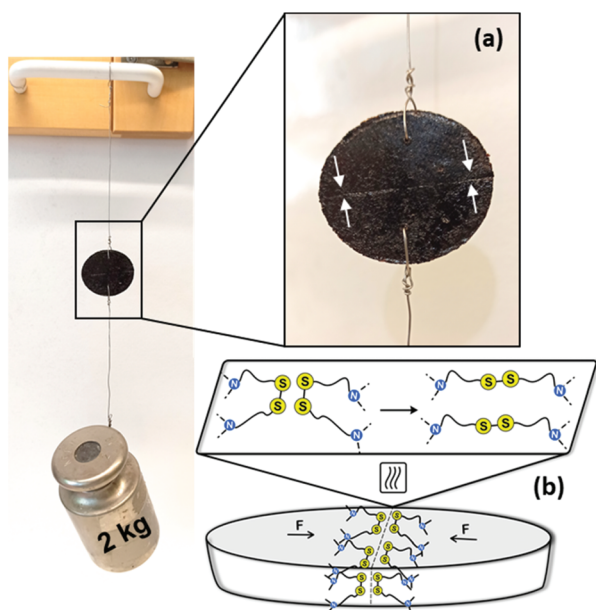

Fig. 6 Healing of the PA CANs. (a) A disk of Cys60 can withstand a 2 kg load after being cut in half and reconnected by pressing and heating the cut surfaces, the white arrows in the enlarged image point the cut; (b) proposed healing mechanism of the sample through heat-activated disulfide exchange at the interface of the two pieces, F denotes the force that keeps the two sides in contact with each other.
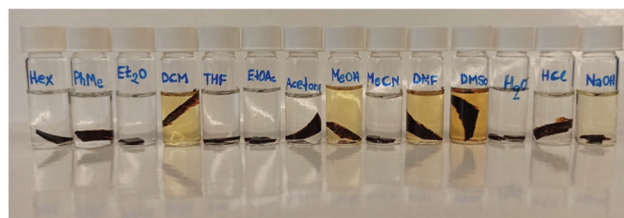

Fig. 7 Chemical resistance of the PA CANs; Cys40 after being immersed in each solvent for 24 h. From left to right: hexane, toluene, diethyl ether, dichloromethane, tetrahydrofuran, ethyl acetate, acetone, methanol, acetonitrile, dimethylformamide, dimethyl sulfoxide, water, hydrochloric acid (aq. 1 M) and sodium hydroxide (aq. 1 M).

CANs were robust materials that can perform in various chemical environments without being considerably affected.

Conclusions

Long-chain, PA associative CANs based on renewable ethylene brassylate were successfully developed by employing disulfide exchange as the dynamic reaction. The structure–property relation of the PA CANs was investigated and the effect of the aliphatic chains and the number of S–S bonds on their properties was elucidated. The networks were reprocessable over three cycles without deterioration of their performance, and demonstrated healing ability by applying an external stimulus. Overall, the system has several sustainable characteristics: (i) it utilizes a renewable resin, (ii) it is devoid of solvents and toxic reagents, (iii) it is easy and simple to handle, (iv) it is quickly healable and (v) it provides the opportunity to prepare fully functional materials from its own 'waste'. These features make the developed long-chain PA CANs highly attractive for applications that require materials with the properties of cross-linked PAs combined with the ability to regain function after damage, through simple mechanical reprocessing and thus, prolonging their service life. The materials presented here are promising candidates for a closed-loop environment where maximum utilization of a material is realized.

Conflicts of interest

There are no conflicts to declare.

Acknowledgements

References

1 Y. Jin, Z. Lei, P. Taynton, S. Huang and W. Zhang, *Matter*, 2019, **1**, 1456–1493.
2 M. Capelot, D. Montarnal, F. Tournilhac and L. Leibler, *J. Am. Chem. Soc.*, 2012, **134**, 7664–7667.
3 Y. X. Lu and Z. Guan, *J. Am. Chem. Soc.*, 2012, **134**, 14226–14231.
4 W. Q. Yuan, G. L. Liu, C. Huang, Y. D. Li and J. B. Zeng, *Macromolecules*, 2020, **53**, 9847–9858.
5 H. Memon, H. Liu, M. A. Rashid, L. Chen, Q. Jiang, L. Zhang, Y. Wei, W. Liu and Y. Qiu, *Macromolecules*, 2020, **53**, 621–630.
6 R. L. Snyder, D. J. Fortman, G. X. De Hoe, M. A. Hillmyer and W. R. Dichtel, *Macromolecules*, 2018, **51**, 389–397.
7 P. R. Christensen, A. M. Scheuermann, K. E. Loeffler and B. A. Helms, *Nat. Chem.*, 2019, **11**, 442–448.
8 M. K. McBride, B. T. Worrell, T. Brown, L. M. Cox, N. Sowan, C. Wang, M. Podgorski, A. M. Martinez and C. N. Bowman, *Annu. Rev. Chem. Biomol. Eng.*, 2019, **10**, 175–198.
9 F. Stempfle, P. Ortmann and S. Mecking, *Chem. Rev.*, 2016, **116**, 4597–4641.
10 P. Ortmann, T. A. Lemke and S. Mecking, *Macromolecules*, 2015, **48**, 1463–1472.
11 M. A. R. Meier, *Macromol. Rapid Commun.*, 2019, **40**, 1–10.
12 N. Kolb, M. Winkler, C. Syldatk and M. A. R. Meier, *Eur. Polym. J.*, 2014, **51**, 159–166.
13 M. Winkler and M. A. R. Meier, *Green Chem.*, 2014, **16**, 3335–3340.
14 P. H. Nguyen, S. Spoljaric and J. Seppälä, *Eur. Polym. J.*, 2018, **109**, 16–25.
15 P. H. Nguyen, S. Spoljaric and J. Seppälä, *Polymer*, 2018, **153**, 183–192.
16 Z. Guo, W. Wang, Y. Yang, K. Majeed, B. Zhang, F. Zhou and Q. Zhang, *Polym. Chem.*, 2021, **12**, 2009–2015.
17 M. Wu, L. Yuan, F. Jiang, Y. Zhang, Y. He, Y. Z. You, C. Tang and Z. Wang, *Chem. Mater.*, 2020, **32**, 8325–8332.
18 L. Song, T. Zhu, L. Yuan, J. Zhou, Y. Zhang, Z. Wang and C. Tang, *Nat. Commun.*, 2019, **10**, 1–8.
19 Y. Chen, A. M. Kushner, G. A. Williams and Z. Guan, *Nat. Chem.*, 2012, **4**, 467–472.
20 D. Montarnal, M. Capelot, F. Tournilhac and L. Leibler, *Science*, 2011, **334**, 965–968.
21 F. Lossada, D. Jiao, X. Yao and A. Walther, *ACS Macro Lett.*, 2020, **9**, 70–76.
22 J. P. Brutman, P. A. Delgado and M. A. Hillmyer, *ACS Macro Lett.*, 2014, **3**, 607–610.
23 D. J. Fortman, R. L. Snyder, D. T. Sheppard and W. R. Dichtel, *ACS Macro Lett.*, 2018, **7**, 1226–1231.
24 J. H. Chen, W. Q. Yuan, Y. D. Li, Y. X. Weng and J. B. Zeng, *ACS Sustainable Chem. Eng.*, 2019, **7**, 15147–15153.
25 S. Dhers, G. Vantomme and L. Avérous, *Green Chem.*, 2019, **21**, 1596–1601.
26 Y. Xu, K. Odelius and M. Hakkarainen, *ACS Sustainable Chem. Eng.*, 2020, **8**, 17272–17279.
27 D. J. Fortman, J. P. Brutman, C. J. Cramer, M. A. Hillmyer and W. R. Dichtel, *J. Am. Chem. Soc.*, 2015, **137**, 14019–14022.
28 F. Elizalde, R. H. Aguirresarobe, A. Gonzalez and H. Sardon, *Polym. Chem.*, 2020, **11**, 5386–5396.
29 M. Röttger, T. Domenech, R. Van Der Weegen, A. Breuillac, R. Nicolaÿ and L. Leibler, *Science*, 2017, **356**, 62–65.
30 O. R. Cromwell, J. Chung and Z. Guan, *J. Am. Chem. Soc.*, 2015, **137**, 6492–6495.
31 M. Delahaye, J. M. Winne and F. E. Du Prez, *J. Am. Chem. Soc.*, 2019, **141**, 15277–15287.
32 F. Cuminet, S. Caillol, E. Dantras, E. Leclerc and V. Ladmiral, *Macromolecules*, 2021, **54**, 3927–3961.
33 E. K. Bang, M. Lista, G. Sforazzini, N. Sakai and S. Matile, *Chem. Sci.*, 2012, **3**, 1752–1763.

34 A. Rekondo, R. Martin, A. Ruiz De Luzuriaga, G. Cabañero, H. J. Grande and I. Odriozola, *Mater. Horiz.*, 2014, **1**, 237–240.

35 J. Dong, B. Liu, H. Ding, J. Shi, N. Liu, B. Dai and I. Kim, *Polym. Chem.*, 2020, **11**, 7524–7532.

36 C. Zhang, H. Liang, D. Liang, Z. Lin, Q. Chen, P. Feng and Q. Wang, *Angew. Chem.*, 2020, **510642**, 4289–4299.

37 M. Bin Rusayyis and J. M. Torkelson, *Macromolecules*, 2020, **53**, 8367–8373.

38 L. Imbernon, E. K. Oikonomou, S. Norvez and L. Leibler, *Polym. Chem.*, 2015, **6**, 4271–4278.

39 M. Chen, L. Zhou, Y. Wu, X. Zhao and Y. Zhang, *ACS Macro Lett.*, 2019, **8**, 255–260.

40 A. Ruiz De Luzuriaga, R. Martin, N. Markaide, A. Rekondo, G. Cabañero, J. Rodríguez and I. Odriozola, *Mater. Horiz.*, 2016, **3**, 241–247.

41 J. H. Chen, D. D. Hu, Y. D. Li, F. Meng, J. Zhu and J. B. Zeng, *Polymer*, 2018, **143**, 79–86.

42 Y. Y. Liu, J. He, Y. D. Li, X. L. Zhao and J. B. Zeng, *Ind. Crops Prod.*, 2020, **153**, 112576.

43 G. Hua and K. Odelius, *Biomacromolecules*, 2018, **19**, 1573–1581.

44 C. Pronoitis, G. Hua, M. Hakkarainen and K. Odelius, *Macromolecules*, 2019, **52**, 6181–6191.

45 X. Y. Jian, X. P. An, Y. D. Li, J. H. Chen, M. Wang and J. B. Zeng, *Macromolecules*, 2017, **50**, 5729–5738.

46 R. Hill and E. E. Walker, *J. Polym. Sci.*, 1948, **3**, 609–630.

47 Y. Kinoshita, *Makromol. Chem.*, 1959, **33**, 1–20.

48 W. G. Perkins and R. S. Porter, *J. Mater. Sci.*, 1977, **12**, 2355–2388.

49 N. S. Murthy, *J. Polym. Sci., Part B: Polym. Phys.*, 2006, **44**, 1763–1782.

50 T. G. Heafield, G. Hopkins and L. Hunter, *Nature*, 1942, **149**, 218.

51 L. M. Gregoret, S. D. Rader, R. J. Fletterick and F. E. Cohen, *Proteins: Struct., Funct., Bioinf.*, 1991, **9**, 99–107.

52 D. L. Howard and H. G. Kjaergaard, *Phys. Chem. Chem. Phys.*, 2008, **10**, 4113–4118.

53 A. Pascual, H. Sardon, A. Veloso, F. Ruipérez and D. Mecerreyes, *ACS Macro Lett.*, 2014, **3**, 849–853.

54 F. Magliozzi, A. Scali, G. Chollet, H. Cramail, D. Montarnal and E. Grau, *ACS Sustainable Chem. Eng.*, 2020, **8**, 9125–9135.

55 J. Meng, Y. Zeng, P. Chen, J. Zhang, C. Yao, Z. Fang, P. Ouyang and K. Guo, *Macromol. Mater. Eng.*, 2020, **305**, 1–8.

56 G. D'escamard, C. De Rosa and F. Auriemma, *AIP Conf. Proc.*, 2016, **1736**, 020176.

57 D. Chan, Y. Ding, R. H. Dauskardt and E. A. Appel, *ACS Appl. Mater. Interfaces*, 2017, **9**, 42217–42224.

58 Y. Gu, J. Zhao and J. A. Johnson, *Trends Chem.*, 2019, **1**, 318–334.

59 C. W. Bunn, *Trans. Faraday Soc.*, 1939, **35**, 482–491.

60 M. P. F. Pepels, M. R. Hansen, H. Goossens and R. Duchateau, *Macromolecules*, 2013, **46**, 7668–7677.

61 P. Ortmann, I. Heckler and S. Mecking, *Green Chem.*, 2014, **16**, 1816–1827.

62 L. Fontana, M. Santoro, R. Bini, D. Q. Vinh and S. Scandolo, *J. Chem. Phys.*, 2010, **133**, 204502.

63 K. Tashiro, S. Sasaki and M. Kobayashi, *Macromolecules*, 1996, **29**, 7460–7469.

64 J. Fernández, H. Amestoy, H. Sardon, M. Aguirre, A. Larrañaga Varga and J. R. Sarasua, *J. Mech. Behav. Biomed. Mater.*, 2016, **64**, 209–219.

65 C. W. Bunn, *J. Polym. Sci.*, 1955, **XVI**, 323–343.

66 K. Saotome and H. Komoto, *J. Polym. Sci., Part A-1: Polym. Chem.*, 1966, **4**, 1463–1473.

67 M. Ehrenstein, P. Smith and C. Weder, *Macromol. Chem. Phys.*, 2003, **204**, 1599–1606.

68 M. Ehrenstein, S. Dellsperger, C. Kocher, N. Stutzmann, C. Weder and P. Smith, *Polymer*, 2000, **41**, 3531–3539.

69 W. Denissen, G. Rivero, R. Nicolaÿ, L. Leibler, J. M. Winne and F. E. Du Prez, *Adv. Funct. Mater.*, 2015, **25**, 2451–2457.

70 M. D. Stern and A. V. Tobolsky, *J. Chem. Phys.*, 1946, **14**, 93–100.

71 W. Ge, B. Zhao, W. Liu, K. Nie and S. Zheng, *Macromol. Rapid Commun.*, 2021, **42**, 2000718.

72 J. Deng, X. Kuang, R. Liu, W. Ding, A. C. Wang, Y. C. Lai, K. Dong, Z. Wen, Y. Wang, L. Wang, H. J. Qi, T. Zhang and Z. L. Wang, *Adv. Mater.*, 2018, **30**, 1–10.

73 A. Takahashi, T. Ohishi, R. Goseki and H. Otsuka, *Polymer*, 2016, **82**, 319–326.

74 Z. Q. Lei, H. P. Xiang, Y. J. Yuan, M. Z. Rong and M. Q. Zhang, *Chem. Mater.*, 2014, **26**, 2038–2046.

75 Y.-R. Luo, *Comprehensive Handbook of Chemical Bond Energies*, CRC Press, Boca Raton, 1st edn, 2007.

76 S. M. Kim, H. Jeon, S. H. Shin, S. A. Park, J. Jegal, S. Y. Hwang, D. X. Oh and J. Park, *Adv. Mater.*, 2018, **30**, 1–8.

77 X. Li, R. Yu, Y. He, Y. Zhang, X. Yang, X. Zhao and W. Huang, *ACS Macro Lett.*, 2019, **8**, 1511–1516.